

Thermodynamic Databases of Nd-Fe-B-Dy Quaternary Alloy Systems and Alloy Design

Wang Cuiping¹, Lu Yong¹, Deng Yuling¹, Guo Yihui¹, Huang Yixiong¹,
Chen Menghua¹, Li Zhou², Liu Xingjun^{1,2}, Liu Guozheng^{3,4}

¹ College of Materials and Fujian Provincial Key Laboratory of Materials Genome, Xiamen University, Xiamen 361005, China; ² Department of Materials Science and Engineering, Harbin Institute of Technology, Shenzhen 518055, China; ³ State Key Laboratory of Baiyunobo Rare Earth Resource Researches and Comprehensive Utilization, Baotou 014030, China; ⁴ Baotou Research Institute of Rare Earths, Baotou 014030, China

Abstract: The CALPHAD method was used to optimize and calculate the phase diagrams of Dy-Nd, B-Dy binary systems and Fe-B-Dy, Dy-Fe-Nd and B-Dy-Nd ternary systems. With taking into account the consistency of the thermodynamic models, the thermodynamic databases of Nd-Fe-B-Dy quaternary alloys were established by the thermodynamic parameters of binary and ternary sub-systems reported in the literature. The longitudinal cross-section phase diagrams of Nd-Fe-B-Dy quaternary alloy $\text{Nd}_{16-x}\text{Dy}_x\text{Fe}_{77}\text{B}_7$ ($x \leq 5$ at%) were predicted by using these databases. At the same time, the variation of the fractions of each phase of the permanent magnet alloy with different Dy contents under equilibrium solidification was analyzed. These results could be helpful for the microstructure design of the Dy-doped NdFeB permanent magnet alloy and the selection of the preparation process parameters.

Key words: Nd-Fe-B-Dy quaternary system; thermodynamic; CALPHAD

The permanent magnet material has the function of mutual conversion between mechanical energy and electromagnetic energy. The permanent magnet material can be made into various forms of permanent magnet functional devices by utilizing its energy conversion function and various physical effects of magnetism. Among them, the rare earth iron-based permanent magnet material consists of the third-generation rare earth metals that have the best magnetic properties (energy density), the widest application and the fastest development speed^[1,2]. The research of NdFeB alloy can not only open up new possibilities for the application of permanent magnet materials, but also greatly accelerate the exploration of new rare earth permanent magnet materials. Permanent magnets of Nd-Fe-B alloy have excellent magnetic properties and

the maximum magnetic energy product (BH) of Nd-Fe-B alloy can reach 240 to 400 kJ/m³, which is known as “the king of the permanent magnets”^[3]. However, the Curie temperature of Nd-Fe-B alloy only ranges from 310 to 510 °C, and the use temperature is only about 80 °C. Their temperature stability and corrosion resistance are quite poor. The actual coercive force is just about 21% of the theoretical value. Therefore, the performance of Nd-Fe-B alloy has large room to be improved^[4,5].

A large number of observations show that the permanent magnet NdFeB alloy generally consists of Nd₂Fe₁₄B phase, Nd-rich phase and B-rich phase^[6].

The heavy rare earth element Dy has a larger magnetic anisotropy field compared to Nd, so replacing the Nd with Dy and supplementing it with appropriate heat treatment

Received date: September 06, 2019

Foundation item: Open Fund of State Key Laboratory of Baiyunobo Rare Earth Resource Researches and Comprehensive Utilization (2017Z1951); National Natural Science Foundation of China (51771158)

Corresponding author: Liu Guozheng, Ph. D., State Key Laboratory of Baiyunobo Rare Earth Resource Researches and Comprehensive Utilization, Baotou Research Institute of Rare Earths, Baotou 014030, P. R. China. E-mail: Lguozheng@163.com

Copyright © 2020, Northwest Institute for Nonferrous Metal Research. Published by Science Press. All rights reserved.

can effectively improve the coercive force of the Nd-Fe-B alloy. The temperature stability and corrosion resistance of the Nd-Fe-B alloy were thus improved^[7, 8]. However, the addition of Dy may cause a sharp drop in the saturation magnetization of the magnet and limit the increase in the maximum magnetic energy product, so the content of Dy should be modulated carefully^[9, 10].

In order to reduce the cost and time-spending during the development of materials, this study aims to establish thermodynamic databases of Nd-Fe-B-Dy quaternary alloys by using the CALPHAD method. Several binary and ternary thermodynamic optimization parameter (Nd-Dy, Dy-B binary systems and Fe-B-Dy, Dy-Fe-Nd, B-Dy-Nd ternary systems) were obtained in this study. The application of the database in the design of rare earth permanent magnet alloy compositions was explored.

1 Thermodynamic Models

1.1 Pure elements

Pure elements are the basis of the CALPHAD thermodynamic databases. The absolute value of their Gibbs free energy is usually undeterminable, the molar enthalpy of the solid phase of the pure component at 298.15 K and 0.1 MPa is defined as the reference state of the stable element (SER: Stable Element Reference), expressed by: H_i^{SER} (298.15 K).

Then the functional relationship of the pure component Gibbs free energy ${}^0G_i^\phi(T)$ at a fixed pressure is expressed as follows:

$${}^0G_i^\phi(T) = G_i^\phi(T) - H_i^{\text{SER}} = a + bT + cT \ln T + dT^2 + eT^3 + fT^{-1} + gT^7 + hT^{-9} \quad (1)$$

where, a, b, c, d, e, f, g and h are model parameters.

In this study, the reference states of pure components Nd, Fe, B and Dy and their Gibbs free energies are derived from the SGTE pure element databases^[11].

1.2 Liquid phase and solid solution phases

The Gibbs free energies of liquid phase and solid solution phases in the binary systems are all described by the sub-regular solution model, expressed as follows:

$$G_m^L = \sum x_i G_i^L + RT \sum x_i \ln x_i + {}^E G_m^L + {}^{\text{mag}} G_m^L \quad (2)$$

where x_i is the molar fraction of i in liquid phase, G_i^L is liquid molar Gibbs free energy of pure element i , R is gas constant, ${}^E G_m^L$ is liquid molar excess Gibbs free energy. ${}^E G_m^L$ is in the form of the Redlich-Kister^[12] polynomial which can be expressed as follows:

$${}^E G_m^L = x_i x_j \left[{}^0 L_{i,j}^L + {}^1 L_{i,j}^L (x_i - x_j) + {}^2 L_{i,j}^L (x_i - x_j)^2 + \dots \right] \quad (3)$$

where ${}^n L_{i,j}^L$ is the interaction parameters between element i and j in liquid phase, and it can be expressed in the following form:

$${}^n L_{i,j}^L = a + bT + cT \ln T + \dots \quad (4)$$

where a, b and c are the parameters to be optimized.

When expanded into the ternary system, the excess Gibbs free energy ${}^E G_m^L$ can be described by the Redlich-Kister-Muggianu^[13] polynomial. Taking the liquid phase in the Dy-Fe-Nd ternary system as an example,

$${}^E G_m^L = x_{\text{Dy}} x_{\text{Fe}} L_{\text{Dy,Fe}}^L + x_{\text{Dy}} x_{\text{Nd}} L_{\text{Dy,Nd}}^L + x_{\text{Fe}} x_{\text{Nd}} L_{\text{Fe,Nd}}^L + x_{\text{Dy}} x_{\text{Fe}} x_{\text{Nd}} L_{\text{Dy,Fe,Nd}}^L \quad (5)$$

$$\text{where } L_{i,j}^L = {}^0 L_{i,j}^L + {}^1 L_{i,j}^L (x_i - x_j) + {}^2 L_{i,j}^L (x_i - x_j)^2 + \dots \quad (6)$$

$i = \text{Dy, Fe, Nd}; j = \text{Dy, Fe, and } i \neq j$.

$$L_{\text{Dy,Fe,Nd}}^L = x_{\text{Dy}} {}^0 L_{\text{Dy,Fe,Nd}}^L + x_{\text{Fe}} {}^1 L_{\text{Dy,Fe,Nd}}^L + x_{\text{Nd}} {}^2 L_{\text{Dy,Fe,Nd}}^L \quad (7)$$

In formula (6), ${}^n L_{i,j}^L$ is the binary interaction parameter between Dy and Fe, Dy and Nd or Fe and Nd in the liquid phase, ${}^n L_{\text{Dy,Fe,Nd}}^L$ is the ternary interaction parameter between Dy, Fe and Nd in the liquid phase. They can be written in the following form:

$${}^n L_{i,j}^L = a' + b'T + c'T \ln T + \dots \quad (8)$$

$${}^n L_{\text{Dy,Fe,Nd}}^L = a'' + b''T + c''T \ln T + \dots \quad (9)$$

where the a', b', c', a'', b'' and c'' are parameters to be optimized.

The term ${}^{\text{mag}} G_m^\phi$ is the magnetic contribution to the Gibbs free energy, which can be expressed by the following expression^[14]:

$${}^{\text{mag}} G_m^\phi = RT \ln(\beta^\phi + 1) f(\tau) \quad (10)$$

The terminal solid solution phases in this study are as follows: fcc phase (γFe), bcc phases ($(\beta\text{Dy}), (\delta\text{Fe}), (\alpha\text{Fe}), (\beta\text{Nd})$), hcp phases ($(\alpha\text{Dy}), (\alpha\text{Nd})$) and Beta-Rhombo phase (B).

1.3 Strict stoichiometric compounds

In some systems, there are some compound phases whose atomic ratios between different components are strictly simple integer ratios. For such strictly linear-stoichiometric compounds, this study describes them by using the sublattice model^[15]. Taking the $\text{Fe}_{17}\text{Nd}_2$ phase in the Fe-Nd binary system as an example, according to the sublattice model, it is divided into two sublattices. The Fe atom and the Nd atom each occupy one lattice, and the molar Gibbs energy of the $\text{Fe}_{17}\text{Nd}_2$ phase can be expressed as follows:

$$\Delta^0 G_r^{\text{Fe}_{17}\text{Nd}_2} = G^{\text{Fe}_{17}\text{Nd}_2} - 17 {}^0 G_{\text{Fe}}^{\text{ref}} - 2 {}^0 G_{\text{Nd}}^{\text{ref}} = a''' + b'''T + c'''T \ln T \quad (11)$$

In formula (11), Fe^{ref} and Nd^{ref} are the reference states of pure Fe and pure Nd, respectively. The values of a''', b''' and c''' can be obtained by the optimization. The linear-stoichiometric compound phases in this study are as

follows: $\text{Fe}_{17}\text{Nd}_2$ phase in the Fe-Nd binary system, Nd_2B_5 , NdB_2 , NdB_4 and NdB_{66} phases in the Nd-B binary system, FeB_2 and FeB phases in the Fe-B binary system, $\text{Fe}_{17}\text{Dy}_2$, $\text{Fe}_{23}\text{Dy}_6$, Fe_3Dy and Fe_3Dy phases in the Fe-Dy binary system, B_2Dy , B_4Dy , B_{12}Dy and B_{66}Dy phases in the B-Dy binary system, $\text{Fe}_2\text{Nd}_3\text{B}_6$, $\text{Fe}_4\text{Nd}_{1.11}\text{B}_4$ and $\text{Fe}_{14}\text{Nd}_2\text{B}$ phases in the Fe-Nd-B ternary system, $\text{BDy}_3\text{Fe}_{16}$, B_2DyFe_2 , B_4DyFe , $\text{B}_3\text{Dy}_2\text{Fe}$, $\text{B}_7\text{Dy}_3\text{Fe}$ and B_4DyFe_4 phases in the B-Dy-Fe ternary system.

1.4 Intermetallic compounds

In this study, a two-sublattice model^[16] was used to describe the intermetallic phase. For the intermetallic phase B_6Dy in the B-Dy binary system, it has a certain solid solubility range, so it is described by a two-sublattice model. Its model can be expressed as $(\text{B})_6(\text{B}, \text{Dy})$. Assuming that the first sublattice is sublattice I and the second sublattice is sublattice II, the expression of the molar Gibbs free energy is as follows:

$$G_m^{\text{B}_6\text{Dy}} = y_{\text{B}}^{\text{II}} G_{\text{B}_6\text{B}}^{\text{B}_6\text{Dy}} + y_{\text{Dy}}^{\text{II}} G_{\text{B}_6\text{Dy}}^{\text{B}_6\text{Dy}} + 0.1429RT(y_{\text{B}}^{\text{II}} \ln y_{\text{B}}^{\text{II}} + y_{\text{Dy}}^{\text{II}} \ln y_{\text{Dy}}^{\text{II}}) + 0.1429y_{\text{B}}^{\text{II}}y_{\text{Dy}}^{\text{II}}L_{\text{B:B,Dy}} \quad (12)$$

In formula (12), y_{B}^{II} and $y_{\text{Dy}}^{\text{II}}$ represent the atomic fraction of B and Dy atoms in the II sublattice, respectively; $G_{\text{B}_6\text{B}}^{\text{B}_6\text{Dy}}$ is the Gibbs energy per mole atom of the hypothetical compound when the sublattice I is completely occupied by B atoms and the sublattice II is occupied by only one of B or Dy. And $0.1429RT(y_{\text{B}}^{\text{II}} \ln y_{\text{B}}^{\text{II}} + y_{\text{Dy}}^{\text{II}} \ln y_{\text{Dy}}^{\text{II}})$ is the Gibbs energy contributed by the ideal mixture entropy to unit $(\text{B})_6(\text{B}, \text{Dy})$, $0.1429y_{\text{B}}^{\text{II}}y_{\text{Dy}}^{\text{II}}L_{\text{B:B,Dy}}$ is the excess Gibbs energy, $L_{\text{B:B,Dy}}$ is the interaction parameter between B and Dy in the sublattice II while the sublattice I is completely occupied by B atoms, and it is still written in the Redlich-Kister^[17] polynomial form:

$$L_{\text{B:B,Dy}} = a'''' + b''''T \quad (13)$$

Where a'''' and b'''' are the parameters to be optimized.

2 Binary System

Thermodynamic parameters for Fe-Nd, B-Nd and B-Fe binary systems were evaluated by Hallemans et al^[18]. This study will use the thermodynamic parameters of the Fe-Nd, B-Nd and B-Fe binary systems evaluated by them. Thermodynamic parameters for Dy-Fe binary system evaluated by Su et al^[19] were also adopted in the present work. In the present study, the thermodynamic parameters of Dy-Nd and B-Dy binary systems were optimized and the phase diagrams of Dy-Nd and B-Dy binary systems were calculated.

The binary Dy-Nd phase diagram was optimized based on the experimental results of Kobzenko et al^[20] and the compiled phase diagrams of Gschneidner et al^[21] which is shown in Fig. 1a. The calculation phase diagram of the Dy-Nd binary system is shown in Fig. 1b.

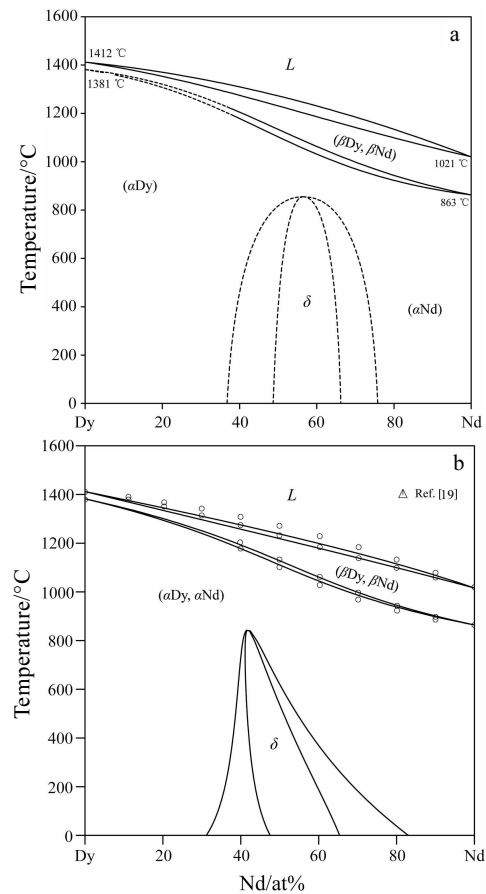


Fig.1 Phase diagram of the Dy-Nd system reviewed by Gschneidner and Calderwood (a) and calculated phase diagram of the Dy-Nd system compared with the experimental data (b)^[20]

The calculated Dy-Nd binary phase diagram in this study was compared with experimental data^[19]. The calculated phase diagram is mostly consistent with the experimental phase diagram^[19], except that the solid solution δ phase is not well reproduced.

The B-Dy binary calculated phase diagram was optimized based on the experimental results of Chaban^[22] et al. and the edited phase diagrams of Etourneau^[23] et al. The calculated phase diagram of the B-Dy binary system is shown in Fig.2.

It can be seen from Fig.2 that the calculated phase diagram is in good agreement with the experimental results. This agreement indicated that the parameters obtained by the optimization well reproduced the previous experimental data.

3 Ternary System

The calculated phase diagram of the Nd-Fe-B ternary system is evaluated by Hallemans^[18] et al. In the present work, the calculated phase diagrams of the Fe-B-Dy,

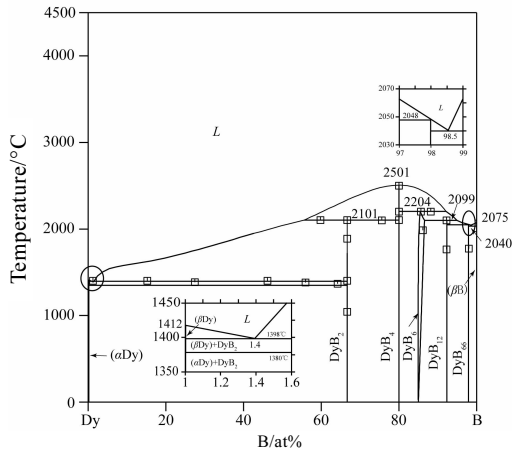


Fig.2 Calculated phase diagram of the B-Dy system with the experimental data^[22]

Dy-Fe-Nd and B-Dy-Nd ternary systems were evaluated.

Using the thermodynamic parameters of the existing B-Dy, B-Fe, Dy-Fe binary systems and the existing experimental phase equilibria of the Fe-B-Dy ternary system, the thermodynamic parameters of the Fe-B-Dy ternary system were optimized and calculated. Fig. 3b shows the isothermal section of the calculated Fe-B-Dy ternary system at 797 °C. Compared with Fig. 3a, the calculated phase diagram is basically consistent with the experimental results. Some experimental data and calculation results have certain discrepancies which are mainly caused by the difference between the evaluation results of the binary sub-systems and the experimental values.

In addition, based on the optimized thermodynamic parameters, the isothermal sections of the Fe-B-Dy ternary system at 400 and 1000 °C are calculated, as shown in Fig. 4a. The calculation results show that some ternary compounds of the system appear as metastable state under different temperature sections, and the three-phase regions and composition ranges are different.

Based on the optimized parameters of Dy-Fe, Dy-Nd and Fe-Nd sub-binary systems, and the experimental phase equilibria reported by Xu et al^[24], the Dy-Fe-Nd ternary system was optimized. The calculated isothermal section at 500 °C is shown in Fig. 5a. Compared with the experimental phase diagram shown in Fig. 5b, the phase equilibrium relationship of the ternary Dy-Fe-Nd at 500 °C is well reproduced. It can be seen from Fig. 5a that the binary linear compounds Fe₂Dy, Fe₃Dy and Fe₂₃Dy₆ have a certain solid solubility of Nd; the composition ranges of [δ + (αDy) + Fe₂Dy] and [δ + (αNd) + Fe₂Dy] in the three-phase equilibrium zone is smaller than that of Xu et al^[24]. This is mainly caused by the difference between the

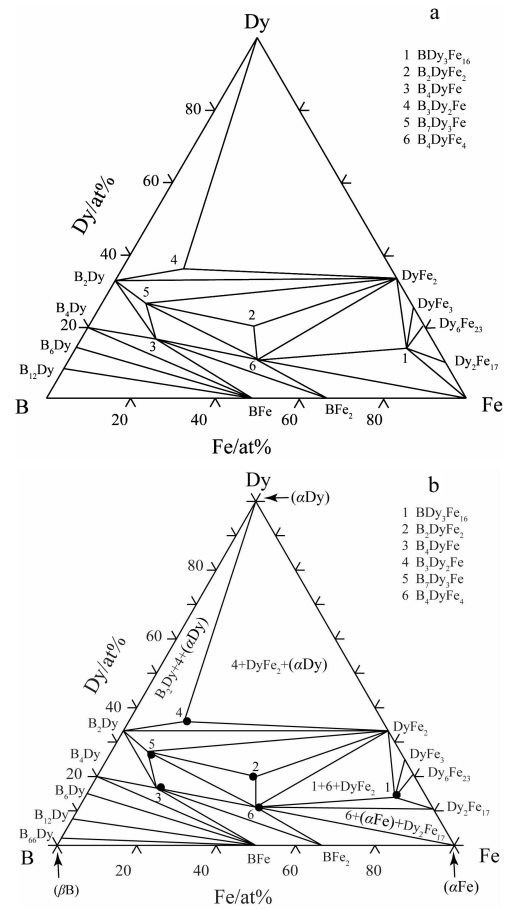


Fig.3 Experiment isothermal section of the Fe-B-Dy system at 797 °C (a) and calculated isothermal section of the Fe-B-Dy system at 797 °C (b)

calculated phase diagram and the experimental data of the Dy-Nd binary system.

The isothermal sections of the Dy-Fe-Nd ternary system at 300, 700, 900 and 1100 °C are shown in Fig 6a~6d, respectively. It can be seen from Fig. 6 that the solubility of Nd element in Fe₂Dy, Fe₃Dy and Fe₂₃Dy₆ phases increases at 300 °C. However the solubility of Nd in the Fe₂Dy, Fe₃Dy and Fe₂₃Dy₆ phases decreases with the increasing temperature. As can be seen from Fig. 6b, the liquid phase firstly appears on the Fe-Nd side from 700 °C, and then the [L + (αNd)] two-phase region appears on the Nd-rich side. When the temperature reaches 900 °C, the liquid phase begins to appear on the Fe-Dy side. In addition, a liquid phase region that runs through the whole temperature range enlarges with the increasing temperature. As shown in Fig. 6c~6d, when the temperatures are 900 and 1100 °C, the three-phase equilibrium zone [L + (αDy) + (αNd)] appears on the Dy-Nd side, and gradually moves toward the Dy-rich side as the temperature rises.

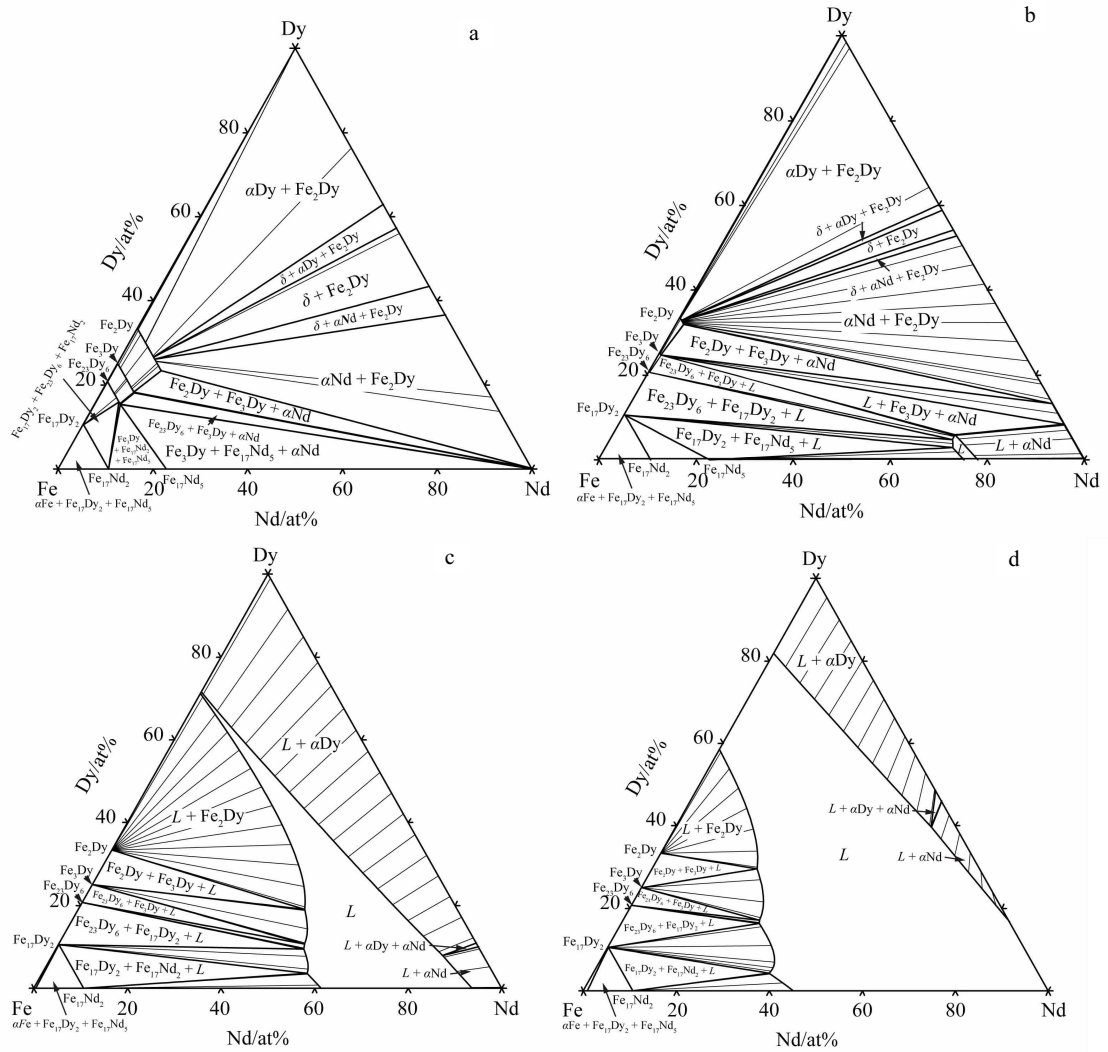


Fig.6 Calculated isothermal section of the Dy-Fe-Nd system at 300 °C (a), 700 °C (b), 900 °C (c), and 1100 °C (d)

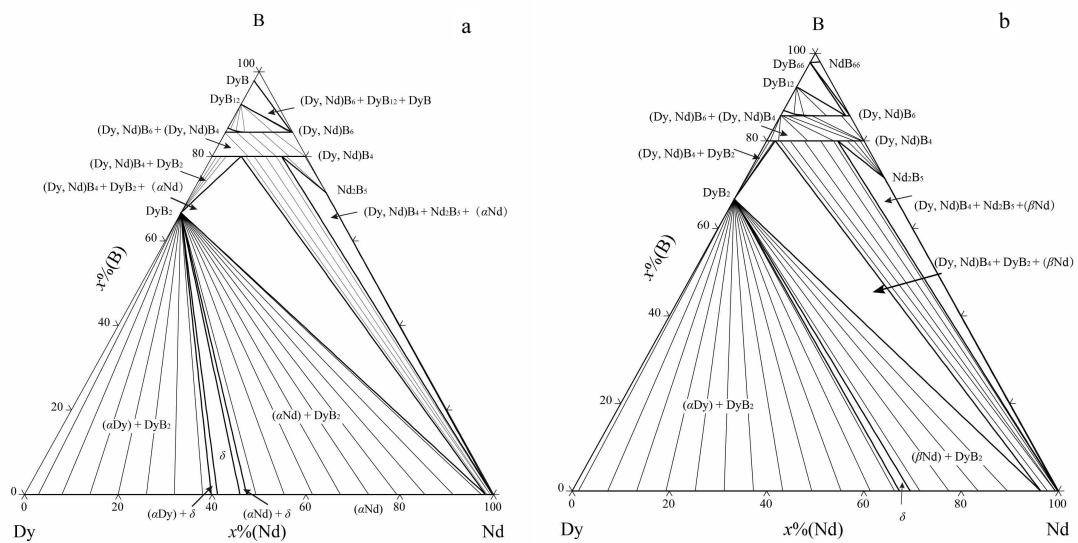


Fig.7 Calculated isothermal section of the B-Dy-Nd system at 700 °C (a) and 1000 °C (b)

Table 1 Thermodynamic assessments of binary and ternary phase diagrams for the Nd-Fe-B-Dy system

Binary systems	Assessment work	Ternary systems	Assessment work
Dy-Nd	This work	Fe-B-Dy	This work
B-Dy	This work	Dy-Fe-Nd	This work
B-Fe	[17]	B-Dy-Nd	This work
B-Nd	[17]	Fe-Nd-B	[17]
Fe-Nd	[17]		
Dy-Fe	[18]		

process curves of the desired system. These calculations could be a good guide for the microstructure design and the selection of preparation process parameters of Dy-doped NdFeB permanent magnet alloy.

The vertical section phase diagram of $\text{Nd}_{16-x}\text{Dy}_x\text{Fe}_{77}\text{B}_7$ ($x \leq 5$ at%) alloy was calculated by the thermodynamic databases of the Nd-Fe-B-Dy quaternary system established in this study, as shown in Fig. 8. It can be seen from Fig. 8 that as the temperature decreases, the hard magnetic phase τ_1 ($\text{Fe}_{14}\text{Nd}_2\text{B}$) and the B-rich phase τ_2 ($\text{Fe}_4\text{Nd}_{11}\text{B}_4$) are precipitated; with the addition of the Dy element, the

compound phases $\text{Fe}_{14}\text{Dy}_2\text{B}$ and Fe_6DyB_4 both appear.

Furthermore, we also calculated the variation of the phase fraction with temperature during equilibrium solidification of the alloys with Dy content of 0, 0.2 at%, 0.4 at%, 1.5 at% and 3 at%, which is shown in Fig 9a~9e.

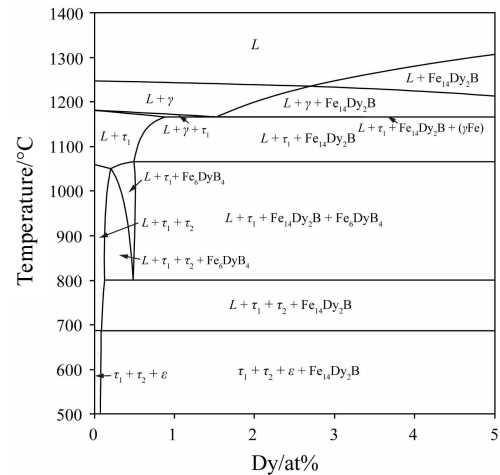


Fig.8 Calculated vertical section phase diagram of the $\text{Nd}_{16-x}\text{Dy}_x\text{Fe}_{77}\text{B}_7$ ($x \leq 5$ at%) alloys

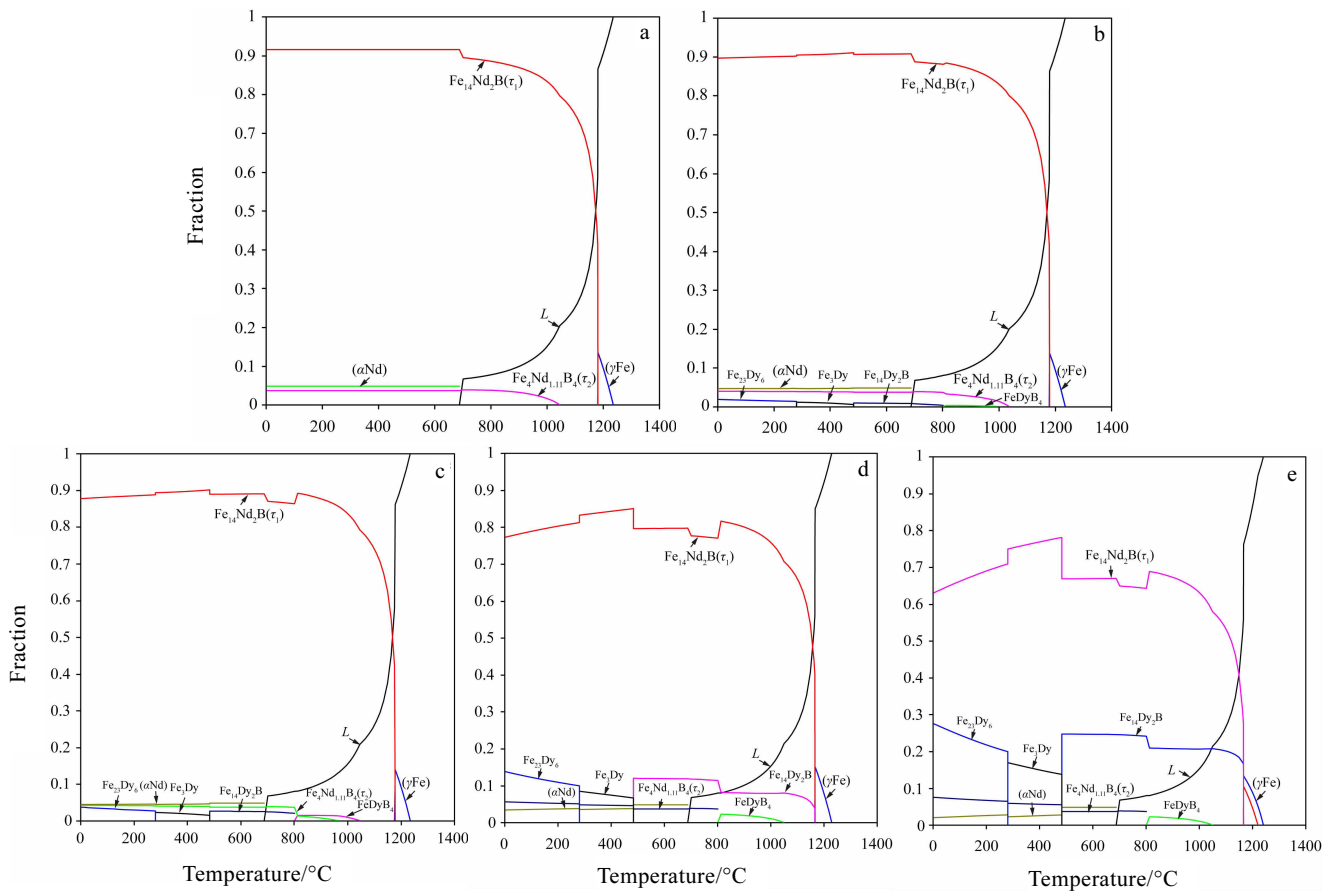


Fig.9 Calculated phase fraction of the $\text{Nd}_{16-x}\text{Dy}_x\text{Fe}_{77}\text{B}_7$ alloy: (a) $x=0$, (b) $x=0.2$ at%, (c) $x=0.4$ at%, (d) $x=1.5$ at%, and (e) $x=3$ at%

As can be seen from Fig. 9a, when $x = 0$, that is, Dy has not been added to the alloy yet, the composition of the alloy is $\text{Nd}_{16}\text{Fe}_{77}\text{B}_7$. When the alloy is in equilibrium and solidified, the (γ Fe) phase firstly forms in the liquid phase; as the temperature decreases, the hard magnetic phase τ_1 and the B-rich phase τ_2 are sequentially precipitated from the liquid phase at temperatures of 1180 and 1044 °C; the region of the liquid phase is gradually reduced. When the temperature drops to 686 °C, the liquid phase disappears and completely transforms into the Nd-rich phase (α Nd); the phase composition of the final alloy is hard magnetic phase τ_1 , rich B phase τ_2 and Nd-rich phase (α Nd), and the corresponding phase fractions are 0.91, 0.04 and 0.05, respectively.

As can be seen from Fig. 9b, when Dy content in the alloy is 0.2 at%, the composition of the alloy is $\text{Nd}_{15.8}\text{Dy}_{0.2}\text{Fe}_{77}\text{B}_7$. During solidification, the hard magnetic phase τ_1 , the B-rich phase τ_2 and the Nd-rich phase (α Nd) gradually precipitate from the liquid phase with the decrease of temperature. In addition, the compound phases Fe_6DyB_4 , $\text{Fe}_{14}\text{Dy}_2\text{B}$, Fe_3Dy and $\text{Fe}_{23}\text{Dy}_6$ phase are formed at temperatures of 991, 800, 482 and 279 °C, respectively. The phase composition of the final alloy is hard magnetic phase τ_1 , rich B phase τ_2 , Nd-rich phase (α Nd) and $\text{Fe}_{23}\text{Dy}_6$ phase, and the corresponding phase fractions are 0.90, 0.04, 0.04 and 0.02, respectively.

From Fig. 9b-9e, it can be seen that when the Dy element is added, a hard magnetic phase τ_1 forms as the temperature decreases. The B-rich phase τ_2 and the Nd-rich phase (α Nd) gradually precipitate from the liquid phase; in addition, the compound phases Fe_6DyB_4 , $\text{Fe}_{14}\text{Dy}_2\text{B}$, Fe_3Dy and $\text{Fe}_{23}\text{Dy}_6$ are formed. As the Dy content increases, the fraction of the Fe_6DyB_4 , $\text{Fe}_{14}\text{Dy}_2\text{B}$, Fe_3Dy and $\text{Fe}_{23}\text{Dy}_6$ phases increase and leads to a continuous decrease in the hard magnetic phase τ_1 . When $x=3$, that is, the content of Dy in the alloy reaches at 3 at%, the phase fraction of the hard magnetic phase τ_1 falls to 63.0%, as shown in Fig. 9e. At the same time, the temperature range in which $\text{Fe}_{14}\text{Dy}_2\text{B}$ phase is stable increases with the increase of Dy content, and the temperature range of Fe_6DyB_4 , Fe_3Dy and $\text{Fe}_{23}\text{Dy}_6$ phase is almost unchanged. When the Dy content is 3 at%, the $\text{Fe}_{14}\text{Dy}_2\text{B}$ phase is precipitated from the liquid phase firstly at 1240 °C.

According to the above calculation results, adding an appropriate amount of Dy will form a new phase with better magnetic properties. It is beneficial to the improvement of the coercive force of the magnet^[7,8]. When element Dy replaces Nd in excess, the new phase excessively formed causes the reduction of the hard magnetic phase τ_1 , and the fraction of the soft magnetic phase rich B phase τ_2 and the Nd-rich phase (α Nd) increase at the same time, resulting in a sharp decrease in the coercive force of the alloy^[9, 25].

5 Summary

1) The thermodynamic parameters of the Nd-Dy and Dy-B binary systems and the Fe-B-Dy, Dy-Fe-Nd and B-Dy-Nd ternary systems were evaluated using the CALPHAD method. The calculated phase diagrams are in good agreement with the experimental phase diagrams.

2) The thermodynamic database of the Nd-Fe-B-Dy quaternary system was established. The phase equilibrium information of the ternary sub-systems at different temperatures in the Nd-Fe-B-Dy system and the vertical section of the $\text{Nd}_{16-x}\text{Dy}_x\text{Fe}_{77}\text{B}_7$ ($x \leq 5$ at%) alloy were calculated.

3) The variation of the fractions of each phase of the permanent magnet alloy with different Dy content under equilibrium solidification was analyzed.

4) The addition of appropriate amount of element Dy causes the formation of a new phase in the alloy which is beneficial for the improvement of the coercive force of the magnet.

References

- Kim A S, Camp F E. *Journal of Applied Physics*[J], 1996, 79(8): 5035
- Davies B E, Mottram R S, Harris I R. *Materials Chemistry and Physics*[J], 2001, 67(1): 272
- Bai G, Gao R W, Sun Y et al. *Journal of Magnetism and Magnetic Materials*[J], 2007, 308(1): 20
- Vial F, Joly F, Nevalainen E et al. *Journal of Magnetism and Magnetic Materials*[J], 2002, 242-245(4): 1329
- Mishra, Raja K. *Journal of Applied Physics*[J], 1987, 61(8): 3778
- Mishra R K. *Journal of Magnetism and Magnetic Materials*[J], 1986, 54: 450
- Zhou S T, Zhang J, Ma D Q et al. *Acta Metallurgica Sinica*[J], 1992, 28(3): B115
- Cheng W H, Li W, Li C J. *Acta Physica Sinica*[J], 2001, 50(1): 139
- Yu L L, Huang C C, Yuan Y F. *Powder Metallurgy Industry*[J], 2009, 18(6): 19
- Yu L Q, Wen Y H, Yan M. *Journal of Magnetism and Magnetic Materials*[J], 2004, 283(2): 353
- Dinsdale A T. *Calphad*[J], 1991, 15(4): 317
- Redlich O, Kister A T. *Ind Eng Chem Res*[J], 1948, 40(2): 345
- Muggianu Y M, Gambino M, Bros J P. *Journal of Materials Engineering and Performance*[J], 1975, 72(1): 83
- Hillert M, Jarl M. *Calphad-computer Coupling of Phase Diagrams & Thermochemistry*[J], 1978, 2(3): 227
- Capdevila C, Caballero F G, García De Andrés C. *Materials Science and Technology*[J], 2003, 19(5): 581
- Harvig H. *Acta Chem Scand*[J], 1971, 25(9): 3199
- Redlich O, Kister A T. *Ind Eng Chem Res*[J], 1948, 40(2): 345
- Hallems B, Wollants P, Roos J R. *Journal of Phase*

- Equilibria*[J], 1995, 16(2): 137
- 19 Su X P, Zhang W J, Du Z M. *Rare Metals*[J], 1999(2): 34
- 20 Kobzenko G F, Svechnikov V M, Martinchuk E L. *Bulletin of Alloy Phase Diagrams*[J], 1972, A(6): 563
- 21 Gschneidner K A, Calderwood F W. *Bulletin of Alloy Phase Diagrams*[J], 1982, 3(3): 348
- 22 Chaban N F, Bilonizhko N S. *Powder Metallurgy and Metal Ceramics*[J], 1994, 32(11): 928
- 23 Etourneau J, Hagemuller P. *Philosophical Magazine B: Physics of Condensed Matter*[J], 1985, 52(3): 589
- 24 Xu H, Huang Y, Li N et al. *Journal of Phase Equilibria and Diffusion*[J], 2015, 36(2): 110

Nd-Fe-B-Dy 四元系热力学数据库的建立及其合金设计

王翠萍¹, 卢勇¹, 邓育灵¹, 郭毅慧¹, 黄艺雄¹, 陈梦华¹, 栗周², 刘兴军^{1,2}, 刘国征^{3,4}

(1. 厦门大学材料学院及福建省材料基因工程重点实验室, 福建 厦门 361005)

(2. 哈尔滨工业大学(深圳)材料科学与工程学院, 广东 深圳 518055)

(3. 白云鄂博稀土资源研究与综合利用国家重点实验室, 内蒙古 包头 014030)

(4. 包头稀土研究院, 内蒙古 包头 014030)

摘要: 本研究利用CALPHAD方法, 采用合理的热力学模型, 热力学优化计算了Nd-Dy、Dy-B二元系和Fe-B-Dy、Dy-Fe-Nd、B-Dy-Nd三元系的相图, 并利用文献报道的其他子二元系和三元系的热力学参数, 充分考虑了热力学模型的一致性和参数的兼容性, 建立了Nd-Fe-B-Dy四元系合金的热力学数据库, 并应用该数据库, 预测了Nd-Fe-B-Dy四元合金 $\text{Nd}_{16-x}\text{Dy}_x\text{Fe}_{77}\text{B}_7$ ($x \leq 5\text{at}\%$)的纵截面相图; 同时还分析了一系列不同Dy含量的永磁合金在平衡凝固下各相相分数随温度的变化情况。这些计算信息对掺NdFeB永磁合金的组织设计以及制备工艺参数的选择具有重要的指导意义。

关键词: Nd-Fe-B-Dy四元系; 热力学; 相图计算

作者简介: 王翠萍, 女, 1963年生, 博士, 教授, 厦门大学材料学院, 福建 厦门 361005, 电话: 0592-2180606, E-mail: wangcp@xmu.edu.cn